Implications of the B20 crystal structure for the magnetoelectronic structure of MnSi

T. Jeong and W. E. Pickett
Department of Physics, University of California, Davis, California 95616, USA
(Received 18 March 2004)

Due to increased interest in the unusual magnetic and transport behavior of MnSi and its possible relation to its crystal structure (B20) which has unusual coordination and lacks inversion symmetry, we provide a detailed analysis of the electronic and magnetic structure of MnSi. The nonsymmorphic $P2_13$ spacegroup leads to unusual fourfold degenerate states at the zone corner R point, as well as "sticking" of pairs of bands throughout the entire Brillouin zone surface. The resulting Fermi surface acquires unusual features as a result of the band sticking. For the ferromagnetic system (neglecting the long wavelength spin spiral) with the observed moment of $0.4\mu_B$/Mn, one of the fourfold levels at R in the minority bands falls at the Fermi energy (E_F), and a threefold majority level at $k=0$ also falls at E_F. The band sticking and presence of bands with vanishing velocity at E_F imply an unusually large phase space for long wavelength, low energy interband transitions that will be important for understanding the unusual resistivity and far infrared optical behavior.

DOI: XXXX PACS number(s): 71.28.+d, 75.10.Lp, 71.18.+y, 71.20.Lp

I. INTRODUCTION

Although the binary compound MnSi has been of interest for some time, unusual behavior of this material has led to accumulating evidence that it is a novel type of weak ferromagnet. MnSi shares the B20 structure with low symmetry occupied sites with the monosilicides of Cr, Fe, and Co that is particularly interesting because of its lack of a center of inversion. Isostructural FeSi has attracted substantial interest as a correlated electron insulator (sometimes referred to as "Kondo insulator") and although the gap of 0.13 eV is reproduced very well by usual density functional based (unpolarized) band theory as shown by Mattheiss and Hamann (MH),[1] a local moment is evident at elevated temperature and correlation effects are obvious. The existence of the gap in band theory seems to be a rather delicate one depending strongly on the internal structural parameters and Fe-Si hybridization, yet the gap persists in (paramagnetic) MnSi where it lies above the Fermi level. Since transition metal silicides (CrSi and CoSi, besides the two mentioned) with varying electron concentrations take this structure, the gap cannot be instrumental in stabilizing this structure.

While FeSi remains paramagnetic in spite of displaying local moment behavior, MnSi becomes magnetically ordered below 29 K. At higher temperatures its susceptibility is Curie-Weiss-like, with a Mn moment of $2.2\mu_B$.[2] It was established by Ishikawa *et al.*[3] that the order is that of a long-wavelength heliomagnet [4] [wavelength $2\pi/q \approx 190$ Å, $q \approx 1/20(\pi/a)$] with an ordered moment of $0.4\mu_B$/Mn. The spiral structure has been attributed to the lack of inversion symmetry in its B20 crystal structure, which brings the Dzyaloshinski-Moriya interaction into play.[5] The Curie temperature drops with pressure until magnetic order disappears[6,7] at the quantum critical point (QCP) of $P_c = 1.46$ GPa, a modest pressure that corresponds to a rather small volume change from ambient pressure. A magnetic field of 1 kOe leads to a conical ordered phase, while 6 kOe is sufficient to transform the system to ferromagnetic (FM) order.[8]

The resistivity $\rho(T)$ under pressure and field has attracted considerable attention. Thessieu *et al.* reported magnetoresistance that showed strong structure in the 0.5–1.2 T range for pressures of 0.7–1.7 GPa.[6] Near the critical pressure P_c, they observed $\rho \propto T^{1.7}$ behavior in zero field that reverted to T^2 at 3.3 T. Initially the resistivity ρ, which is Fermi-liquid-like (T^2) in the FM phase, was reported to be linear-in-T for $P > P_c$,[7] but recent data show it to be $\rho \propto T^{3/2}$ up to 30 kbar (twice P_c).[9] This scaling suggests something different from both normal Fermi liquid behavior ($\rho \propto T^2$) and the T-linear non-Fermi-liquid dependence seen in several metals near the quantum critical point, and nonuniversal. Recent zero-field ^{29}Si NMR data[10] have been interpreted in terms of an onset of inhomogeneous magnetism at 1.2 GPa which extends at least to 1.75 GPa, completely encompassing the QCP. Earlier Thessieu *et al.* had reported,[11] also from ^{29}Si NMR studies, that some kind of local magnetic order remained above P_c. For strong inhomogeneity, such as in a two-phase system, non-Fermi-liquid behavior in $\rho(T)$ would not be so surprising.

There are other data that suggest unusual correlated electron behavior (magnetic fluctuations, presumably) for MnSi. The field dependence of the muon spin relaxation rate reported by Gat-Malureanu *et al.*[12] requires an unconventional explanation. In addition, the optical conductivity even at ambient pressure is strongly non-Drude-like, with the behavior having been represented by Mena *et al.* in terms of a frequency-dependent effective mass.[13] The measured complex low frequency optical conductivity has been modeled by the form $\sqrt{\gamma(T)+i\omega}$, where $\gamma(T)$ is the T-dependent relaxation rate. The antisymmetric part of the magnetic susceptibility that appears due to the non-centrosymmetric space group has recently been measured by Roessli *et al.*[14] The fluctuations well above T_c are incommensurate with the lattice, and furthermore are chiral in nature, meaning that the fluctuation spectrum depends on the sign of the polarization with respect to the momentum transfer $(\vec{P}_{\rm pol}\cdot\vec{Q})$.

As mentioned above, MnSi shares the B20 crystal structure with FeSi, but contains one electron less per formula

unit. In spite of the strong interest in this unique compound, there has been no thorough study of its electronic and magnetic structure in general, and in particular how it relates to the B20 crystal structure. The paramagnetic bands and density of states were presented in a short report by Nakanishi *et al.*[15] Taillefer and collaborators applied the linear muffin-tin orbital method with band shifting to model the Fermi surfaces,[16] but did not report the general electronic structure and magnetic behavior. Trend studies of several transition metal monosilicides using a planewave pseudopotential method were reported by Imai *et al.*[17] Yamada and coworkers have reported studies of the volume dependence of the magnetic moment using the linear muffin-tin orbital method in the atomic sphere approximation.[18,19]

In this paper we present a detailed investigation of the electronic structure and magnetization of MnSi within the local density approximation (LDA) using self-consistent full potential methods. We address specifically the connection of the electronic and magnetic structure to the unusual coordination of the Mn atom and to the nonsymmorphic B20 space group which has no inversion operation. We find that "band sticking" around the faces of the Brillouin zone have consequences for the electronic structure and Fermi surfaces that should be recognized when interpreting data. The LDA minimum of energy occurs for a ferromagnetic moment of almost $1\mu_B$/Mn, considerably higher than the experimental value of $0.4\mu_B$ and also quite different from the value of $0.25\mu_B$ reported earlier by Taillefer, Lonzarich, and Strange[16] with a more approximate method of calculation. Fixing the moment at the observed value, we report the resulting Fermi surfaces. In the minority band, considerable potential for nesting arises. The manner in which these features may influence the observed properties of MnSi are discussed. The equation of state was calculated earlier by Lerch and Jarlborg.[20]

II. THE B20 CRYSTAL STRUCTURE

One view of the MnSi B20 structure is shown in Fig. 1. There are four MnSi formula units in the cubic primitive cell. MH have described in detail how the local coordination of an individual Mn or Si atom can be pictured in terms of an underlying rocksalt unit cube containing four formula units. Starting from the rocksalt idealization, one considers a dimerizing-type distortion involving displacement of Mn or Si atoms along [111] directions, whose primary effect is to transform rocksalt Mn-Si neighbors along [111] directions into MnSi nearest neighbors. These distortions are large (1.6 eV energy gain per molecule calculated by MH), and strongly distort the space-group symmetry from $Fm3m$ to $P2_13$, a primitive lattice generated by a screw axis 2_1 and a threefold axis (3). The Bravais lattice remains simple cubic but the point symmetry is reduced to four threefold axes. The space group consists of threefold rotations around one specific $\langle 111\rangle$ direction, three screw axes consisting of a 180° rotation around a cubic axis followed by a $(\frac{1}{2},\frac{1}{2},0)a$ type nonprimitive translation, and combinations of these.

Both the Mn and Si atoms are located at the $4(a)$-type sites in the simple-cubic unit cell, with position coordinates at $(u,u,u),(\frac{1}{2}+u,\frac{1}{2}-u,-u),(-u,\frac{1}{2}+u,\frac{1}{2}-u)$, and $(\frac{1}{2}-u,-u,\frac{1}{2}+u)$. The corresponding values for the internal atom-position parameters are $u_{\mathrm{Mn}}=0.137$ and $u_{\mathrm{Si}}=0.845$. Given the MnSi lattice parameter is $a=4.558$ Å,[15] the local coordination of Mn consists of one Si neighbor at 2.11 Å (lying along a [111] direction, three neighbors at 2.35 Å and three neighbors at 2.69 Å). The point symmetry at the Mn and Si sites is C_3. Taking into account time-reversal symmetry (when nonmagnetic) with the twelve space group operations, the irreducible Brillouin zone (BZ) is 1/24 of the full zone.

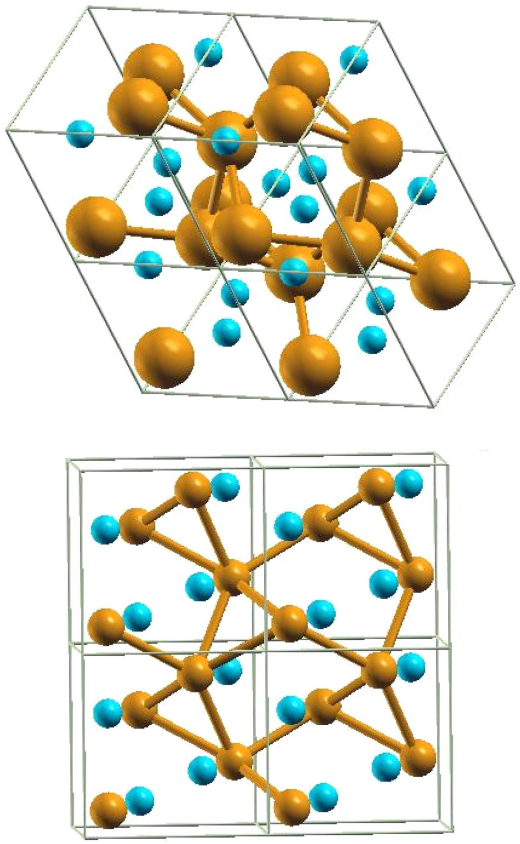

FIG. 1. (Color online) Two views of the B20 crystal structure of MnSi, showing four cubic cells. The larger atoms are Mn and are connected by sticks; the smaller spheres are Si atoms. Top: a view along the (111) direction. Bottom: view nearly along the (100) axis.

Another way to picture the B20 structure has been discussed by Vočadlo *et al.*[21] in terms of an "ideal B20" structure with $u_{\mathrm{Mn}}=1/(4\tau)=0.1545$, $u_{\mathrm{Si}}=1-1/(4\tau)=0.8455$, where $\tau=(1+\sqrt{5})/2$ is the golden ratio. The nearest neighbor coordination of each atom then is seven equidistant atoms of the opposite kind, at a distance $a\sqrt{3}/(2\tau)$. These seven atomic sites lie on seven of the twenty vertices of a pentagonal dodecahedron centered on the atom. This sevenfold coordination also supports the interpretation of Dmitrienko that the B20 structure can be viewed[22] as a crystalline approximation to an icosahedral quasicrystal. To our knowledge, there has been no clear interpretation in terms of chemical bonding of why MnSi (and CrSi, FeSi, CoSi) prefer the B20 structure. Vočadlo *et al.* have calculated[23] the equation of state for FeSi in the B20, NaCl, CsCl, NiAs, and inverse-NiAs structures using the VASP planewave code. They find that under pressure the internal coordinates move closer to

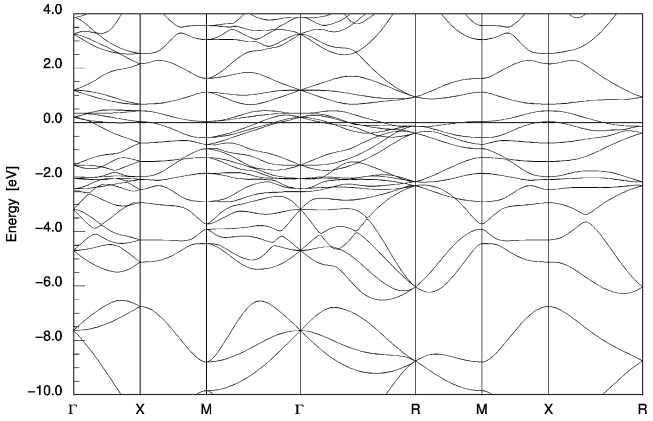

FIG. 2. The full band structures of paramagnetic MnSi along symmetry lines. There is a narrow gap in the bands ~0.6 eV above the Fermi level, corresponding to a band filling of four extra electrons. Bands from −3 to +1 eV are primarily Mn 3*d* character.

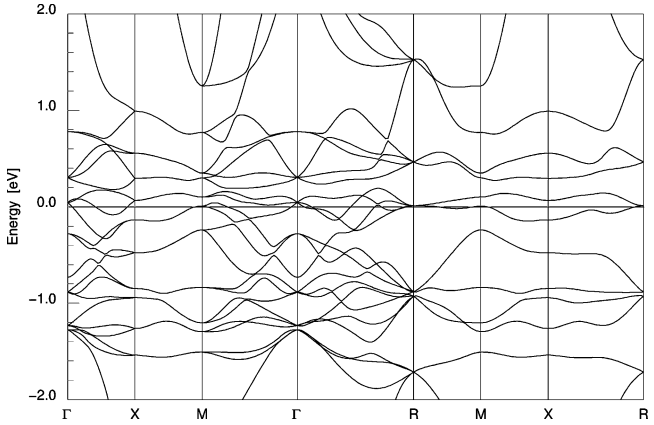

FIG. 3. Plot along symmetry directions of the bands of Mn□, that is, Mn atoms in the observed MnSi B20 structure but with Si atoms missing. The amount of dispersion gives an impression of the "intrinsic" 3*d* bandwidth, while comparison with the full band structure in Fig.2 indicates the considerable shifting of bands due to Si interaction with Mn; for example, at Γ in MnSi, there are no states in the −1.5 to 0.3 eV region.

their ideal values discussed above, and that a transformation to the CsCl structure is predicted at 13 GPa, far above the quantum critical point where magnetism vanishes.

III. METHOD OF CALCULATIONS

We have used the full-potential nonorthogonal local-orbital (FPLO) method[24] within the local density approximation (LDA).[25] Mn $3s,3p,4s,4p,3d$ states and Si $3s,3p,3d$ were included as valence states. All lower states were treated as core states. The inclusion of the relatively extended $3s,3p$ semicore states as band states was done because of the considerable overlap of these states on nearest neighbors. This overlap would otherwise be neglected in the FPLO scheme. Si 3*d* states were added to increase the quality of the basis set. The spatial extension of the basis orbitals, controlled by a confining potential $(r/r_0)^4$, was optimized to minimize the total energy. The self-consistent potentials were carried out on a $20\times20\times20$ uniform mesh in the Brillouin zone, which corresponds to 700*k* points in the irreducible part for $P2_13$.

IV. RESULTS AND DISCUSSIONS

A. Paramagnetic bands

Considering the B20 structure as derived from the rocksalt structure, the MnSi bands look very similar to those presented by MH for FeSi, in both the primitive cell and for the unit cube in which the *X* points are folded back to the Γ point. As noted by MH, there is no reason to expect any Fermi surface driven instability of the rocksalt structure, because several transition metal monosilicides with different band fillings have the same structure. We calculate the B20 structure to be 1.5 eV per formula unit lower in energy than the rocksalt structure. Because of some symmetry-related peculiarities of the band dispersion, we compare the paramagnetic band structure of MnSi with those of rocksalt MnSi as well as to those of the Mn skeleton itself.

Full bands of MnSi. We first show the full bands of MnSi in the valence-conduction region in Fig. 2. It is this PM band structure (at slightly reduced volume) that becomes relevant at the quantum critical point. Since Si contributes four, and Mn contributes seven, valence electrons, there are enough electrons to fill 11×4 molecules/2 spins=22 bands. With the four $3s,3p$ states of Si and the five 3*d* states of Mn, there are 36 bands valence-conduction bands. The lowest four bands in the range −6.5 to −11 eV (see Fig. 2) are Si 3*s* bands. Mn 3*d* character is confined primarily to the −3 to +1 eV region, nevertheless these bands are strongly affected by the mixing with Si (see below). As a result of the Mn *d* -Si *p* interaction, the Si 3*p* character is repelled strongly to the region −3 to −6 eV in the valence bands, and above 1 eV in the conduction bands.

A very narrow indirect gap of 0.1 eV lies just above the Fermi level, as reported earlier by Nakanishi *et al.*[15] This gap, which is the fundamental gap in semiconducting FeSi, occurs above the MnSi Fermi level since this system contains four fewer valence electrons per unit cell. This gap acquires some significance in establishing the stability of the FM state, at least within LDA (see below).

Mn□. To give an impression of Mn bands undisturbed by Si *p* states, and therefore an indication of direct Mn *d*-*d* coupling, we show in Fig. 3 the bands of Mn□ ≡ MnSi with the Si atoms missing. The 3*d* bands are about 2 eV wide at $k=0$ (the density of states extends over 2.5 eV). As is the case also for MnSi itself (Fig. 2), bands "stick together" in pairs along the BZ edges *R*-*X*-*M*-*R*. This symmetry-dictated band-sticking (discussed more fully below) and hybridization make the dispersion appear small along the BZ faces, but the bands emanating radially (along Γ-*X* and Γ-*R* directions) reflect the actual dispersion. At Γ the twenty states (four atoms × five 3*d* states) break up into a single nondegenerate state, two twofold degenerate, and five threefold degenerate states. At the zone corner *R* point, all bands show unusual fourfold degeneracy, again a consequence of the nonsymmorphic nature of the B20 space group.

The zone-edge bands show one other unusual feature. The twenty bands break up into a single sticking pair at the bot-

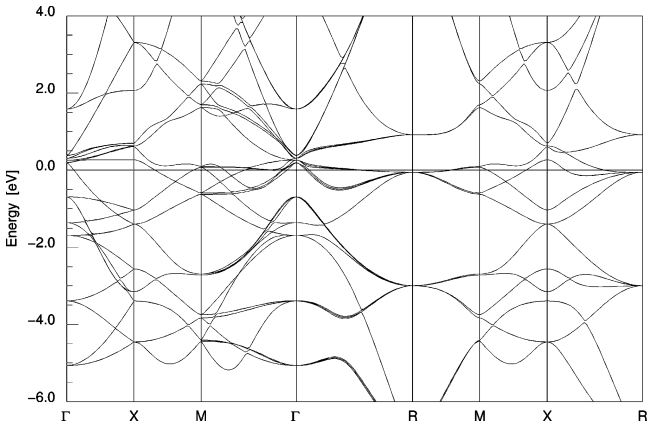

FIG. 4. Band structure for nonmagnetic MnSi in the simple cubic four-molecule nonprimitive cell of the reference rocksalt structure MnSi. Actually, both Mn and Si have been displaced by $\delta u = 0.0025$ to the B20 structure to illustrate lifting of degeneracies (the tiny band splittings, especially at Γ and M) by the crystal symmetry breaking. Note that there is no splitting whatsoever at the zone corner R point, while fourfold degeneracies at X and M are broken into "sticking" pairs.

tom and the top, and into pairs of sticking pairs from −1.5 to 0.5 eV that are disjoint all around the Brillouin zone boundary. Interaction with the Si 3p states completely destroys this simplicity, (Fig. 2) even though rather little Si 3p character remains in these bands.

Rocksalt MnSi. For MnSi in the reference rocksalt structure, the bands in the −6 to 4 eV range are shown in Fig. 4. The Mn and Si positions have been displaced slightly from the rocksalt structure toward the B20 structure: instead of using $u_{\mathrm{Mn}}=0.25, u_{\mathrm{Si}}=0.75$ which would be rocksalt, the values $u_{\mathrm{Mn}}=0.2475$, $u_{\mathrm{Si}}=0.7475$ were used to give some impression of the band splittings that occur for small distortion toward the B20 structure. (This distortion is only about 2% of that needed to produce the actual B20 structure. The MnSi B20 "distortion" is so large that the broken symmetries cannot be located just from the B20 band structure.)

A very flat band around the R point lies almost at E_F, and flat bands lie 0.3 eV above E_F along Γ-X and very near E_F along Γ-M. The occurrence of flat bands is not uncommon is cubic structures, where certain d-d hopping amplitudes can vanish by symmetry. The distortion can be seen to split degeneracies and thereby give vanishing velocities at the M point, and this does not occur at the X point. In the MnSi bands of Fig.2, it is evident that bands along Γ-X hit the X point with nonzero velocity (in fact, pairs of bands hit X with equal magnitudes but opposite sign of their velocity), whereas all bands are flat at the M point.

B. Digression on band sticking

To understand better the extensive band sticking noted in the previous subsection, and because we will encounter fine structure in the band structure at E_F in the (physical) FM case in the next subsection, it is worthwhile to digress briefly to consider the origin of the band sticking phenomenon. Perhaps the most accessible description of the origins of band sticking can be found in the recent papers of König and Mermin. [26,27] Band degeneracy at a wave vector $\vec{k}$ is associated with the little group of $\vec{k}$, which is the subgroup of the point group operations $\{g\}$ that bring $\vec{k}$ back to itself, each modulo a reciprocal lattice vector $\vec{G}_g$. General (nonsymmetric) points on the face of the BZ of the $P2_13$ space group have a little group containing only the identity. To obtain the full symmetry of the actual band structure, we have to augment the symmetry considerations to include time reversal $\mathcal{T}$, whose effect is $\mathcal{T}\psi_k(r)=\psi_{-k}(r)$, i.e., its effect is to invert the wave vector $\mathcal{T}\vec{k}=-\vec{k}$ just as would an inversion operation (which is missing from $P2_13$). Thus in the operations on $\vec{k}$, we include $\mathcal{T}$ together with the actual point group operations.

Consider a point on the BZ face $\vec{K}=(\pi,k_y,k_z)$ (taking unit lattice constant). Now the little group of $\vec{K}$ consists of the identity $\mathcal{I}=g_1$ and the product $\mathcal{T}S=g_2$, where S is the 180° rotation around the $\hat{x}$ axis $(x,y,z)\rightarrow(x,-y,-z)$. When combined with the nonprimitive translation $\tau=(1/2,1/2,0)$, it forms the screw axis space group operation $\mathcal{S}=[S;\tau_S]$. With two members in the little group together with the phase factor introduced by τ for the g_2 operation, the analysis of König and Mermin indicates band sticking over the entire $k_x=\pi$ face (and thus all faces) of the BZ. Explicit calculation confirms the band sticking. The extensive fourfold degeneracy at R that was pointed out in the previous subsection arises already in the rocksalt supercell of Fig.4. Extra degeneracies are expected when a supercell (nonprimitive cell) is chosen; it is a consequence of the $P2_13$ symmetry that these degeneracies remain after the rocksalt →B20 internal distortion.

At the zone corner R point, the little group consists of all space group operations, often refereed to as "full symmetry of the Γ point." In fact, most of the little group members of the R point are associated with nonzero reciprocal lattice vectors $\vec{G}_g$ (unlike the Γ point case), and associated sticking leads to more degeneracy than occurs at the Γ point.

C. Ferromagnetic phase

Since the long wavelength helical magnetic structure can be considered to be locally FM, and a field of only 6 kOe is sufficient to drive the heliomagnetic structure to FM order, it is relevant to consider a simple FM ordering. Since spin-orbit coupling is small in 3d magnets, we neglect it, so the direction of magnetic polarization is not coupled to the lattice. Within LDA, a FM state with moment almost at the half metallic value of $1\mu_B$/Mn is obtained: the Fermi level in the minority bands lies just at the bottom of the gap in the majority bands. The four holes compared to FeSi lie entirely in the minority states. This result is substantially different from experimental moment of $0.4\mu_B$/Mn, and overestimate that is not uncommon for weak ferromagnets near the quantum critical point. It does, however, mean that analyzing the LDA minimum is unfruitful.

To reveal the electronic and magnetic structure of MnSi as fully as possible, we have constrained the moment to the experimental value of $0.4\mu_B$/Mn. The bands in the 3d region

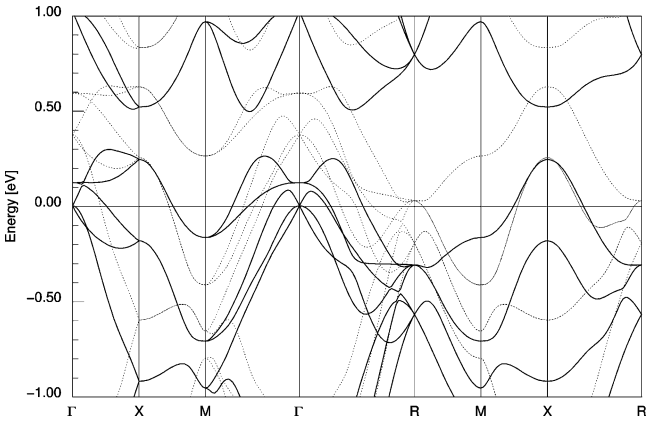

FIG. 5. The bands of ferromagnetic MnSi within 1 eV of the Fermi level when the moment is fixed at the experimental value of $0.4\mu_B$/Mn. Solid lines denote majority bands; dotted lines show minority bands. The exchange splitting in this region is fairly uniform at 0.40±0.03 eV. Note that a fourfold degenerate level in the majority bands falls precisely at the Fermi level, and a fourfold minority state at R lies very close to E_F.

are shown in Fig. 5. The corresponding total and atom-projected densities of states are pictured in Fig. 6, where the predominance of Mn $3d$ character near E_F is evident. The exchange splitting $\Delta_{\mathrm{ex}}=0.4$ eV is rather uniform over the zone, as expected for bands which are of fairly uniform character (Mn $3d$). Identifying $\Delta_{\mathrm{ex}}=Im$ gives a Stoner constant $I\sim 1$ eV/μ_B, a value near the top of the range occurring in $3d$ magnets.

The FM bands are nearly uniformly split versions of the paramagnetic bands. The notable feature is the coincidence of two complexes of degenerate bands at high symmetry points that lie essentially at the Fermi level. (Since the magnetization has not been determined to any more accuracy than "$0.4\mu_B$/Mn" there is an uncertainly of several tens of meV of band placements.) At $k=0$, a threefold level lies precisely at E_F. The middle of these three bands approaches $k=0$ with vanishing slope, while the other two have nonvanishing (equal and opposite in sign) velocities of 1.25×10^7 cm/s. At the zone corner R point, a fourfold level lies extremely near E_F (about 15 meV above). These bands all have vanishing velocity at R.

The occurrence of a vanishing velocity at E_F has a variety of possible consequences which have been discussed at length in the high temperature superconductors,[28,29] and the associated van Hove singularities have great general importance.[30] The most well known case is the half-filled square lattice with only nearest neighbor hopping, where a van Hove singularity occurs at the zone edge $X=(\pi/a,\pi/a)$ point in two dimensions. In addition to causing the van Hove nonanalyticity (and peak) in the DOS, this situation represents the point of change in topology of the Fermi surface, which includes a "Lifshitz anomaly of order $21/2$" in thermodynamic properties[31–34] at low temperature.

D. Fermi surfaces

The Fermi surfaces for a magnetization of $0.4\mu_B$/Mn are shown in Figs. 6–8 for majority and minority spins, respectively. The majority surfaces consist of a Γ-centered rounded octahedron and a pair of open jungle gym type surfaces. These latter two surfaces illustrate two consequences of the unusual B20 space group of MnSi. First, although the Bravais lattice is simple cubic, the lack of a fourfold rotation around the cubic axes is reflected in the elliptical (rather than circular) intersection of the arms with the zone faces. The orientation of the major axis of this ellipse rotates from face to face in a way that preserves the threefold rotation symmetry around ⟨111⟩ axes.

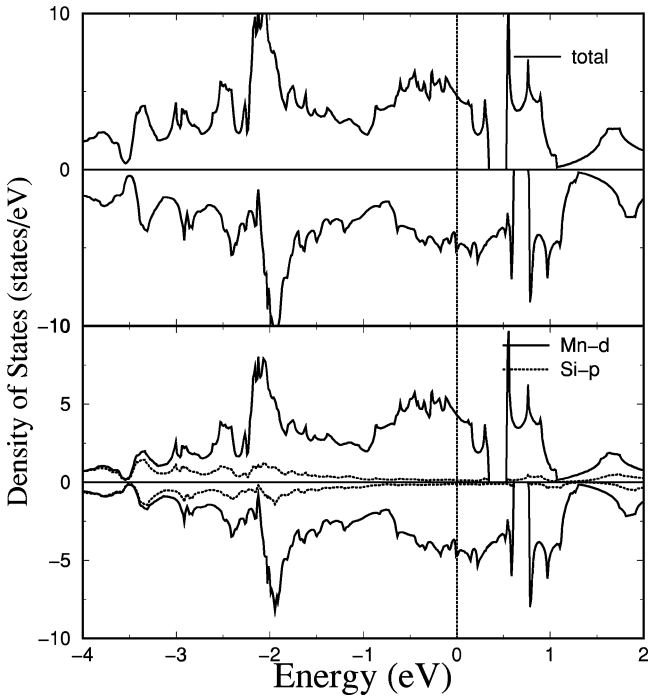

FIG. 6. Projected density of states of ferromagnetic MnSi. Top panel: total, plotted positively for majority, negatively for minority. The near rigid-band shift of states within 1 eV of the Fermi level is evident. Bottom panel: projection of the Mn $3d$ and Si $3p$, showing that Mn $3d$ character dominates the states near Fermi level.

More difficult to accommodate with our conception of periodic cells (whether in real or reciprocal space) is the recognition that these jungle gym arms do not intersect the zone faces perpendicularly. The periodicity of the total Fermi surface is restored by the fact that there are two touching Fermi surfaces on these zone faces (in this case, the two jungle gyms) guaranteed by the sticking together of bands discussed in the previous section. At a given point on the Fermi surface at a zone face, one surface intersects the face at an angle $\pi/2-\theta$ and the other at an angle $\pi/2+\theta$: each Fermi surface connects smoothly to the *other* Fermi surface in the neighboring zone. As a result, the open magneto-oscillation orbits on these surfaces may have behavior different from what is expected from the reciprocal lattice periodicity. In addition, extremal neck orbits do not automatically encircle the X point as is commonly the case (see Fig. 6).

The minority Fermi surfaces, shown in Fig. 7 consist of Γ-centered cube and two jungle gyms (again, stuck together along the zone faces) and appear to be direct analogs of the majority surfaces. There are also two small R-centered ellip-

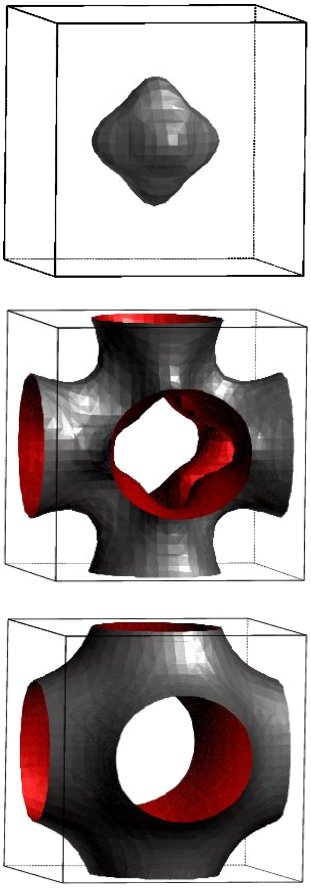

FIG. 7. (Color online) Majority spin Fermi surfaces (from top, bands 37, 38, 39) for a fixed moment equal to the experimental value of $0.4\mu_B$/Mn. The close juxtaposition of the lower two panels illustrate how the smooth connection from one jungle gym surface to the other in a neighboring zone proceeds without the surfaces being perpendicular to the zone face.

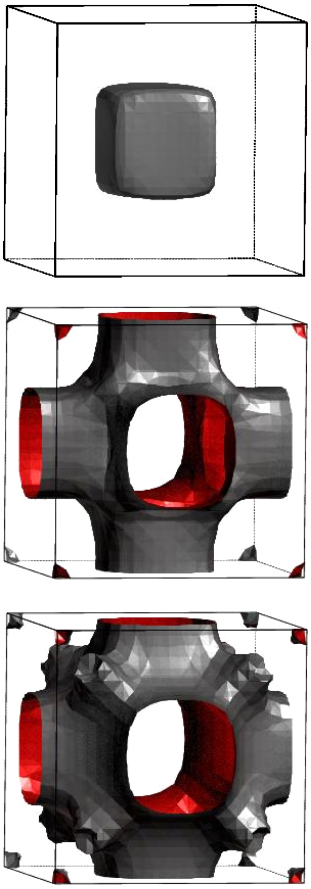

FIG. 8. (Color online) Minority spin Fermi surfaces as in Fig.6 (from top, bands 35, 36, 37). The strong nesting features (top two panels) are discussed in the text. Note that the band 37 jungle gym has additional structured protrusions along the $\langle 111 \rangle$ directions. Two very small hole ellipsoids lie at the zone corner R point.

soids that are not well resolved in Fig. 7. The resemblance of the jungle gyms to those of the majority band (Fig. 6) is largely accidental. As mentioned in the previous section, the spin splitting if nearly uniform at 0.4 eV, so the Fermi level produces a cut in two different regions, which are ±0.2 eV from the paramagnetic Fermi level. The intersections of the jungle gym surfaces with the zone faces can be seen to arise from majority and minority bands which have, apparently accidentally, nearly the same shape along *M*-*X*-*R* in Fig. 5. The similarity in shape of the jungle gym surfaces (for either spin direction) may be understood simply by the fact that they are required by symmetry to "stick" along each of the zone faces, and they do not extend too far away from the faces.

The minority surfaces in particular present a great deal of potential for nesting, as represented, for example, in the quantity

$$\xi(\vec{q}) = \sum_{\vec{k}} \delta(\varepsilon_{\vec{k}+\vec{q}} - \varepsilon_F)\,\delta(\varepsilon_{\vec{k}} - \varepsilon_F) \qquad (1)$$

that measures the number of transitions on the Fermi surface involving momentum transfer $\vec{q}$. Taken together, the cube and the more jungle gym in the center panel of Fig.7 arise from a set of parallel flat ribbons oriented along each of the three Cartesian directions to form intersecting square tubes (somewhat rounded). The dimension across the tube, hence the nesting wave vector, is $Q \approx 0.4(2\pi/a)$. Due to the flat nature of the surfaces, nesting vectors are of the general form $\vec{q}=(q_x, Q, 0)$ and $\vec{q}=(q_x, 0, Q)$ for arbitrary q_x, and others related by cubic symmetry. [We say cubic symmetry rather than the strictly correct "B20 symmetry" because the departure of the shapes of the minority surface from cubic symmetry seems to be less than for the majority jungle gyms.]

We leave a more detailed study of nesting and q dependence of scattering processes for subsequent work. A few other possibilities can be noted, however. The majority octahedron may provide some nesting across the octahedron "faces," that is, for q along the $\langle 111 \rangle$ directions, but they do not appear to be extremely flat. In addition, the sticking together of the jungle gym surfaces all over the zone faces provides substantially larger phase space for $q \to 0$ transitions than for conventional Fermi surfaces and deserves further study. [The trivial *intraband* $1/q$ divergence[35] is a different matter, and is usually killed by intraband matrix elements.]

V. DISCUSSION

The fundamental questions underlying the unusual and perhaps unique characteristics of MnSi center on (1) its unusual bonding and coordination, identical to that of the "Kondo insulator" FeSi, which is related to (2) its low symmetry but still cubic B20 space group in which 75% of the rotations are coupled with a non-primitive translation, and (3) its lack of inversion center (also an integral part of the space group). Frigeri *et al.* have argued, for example, that lack of inversion symmetry in the MnSi space group acts as a strong inhibition[36] to spin triplet pairing (but does not totally exclude it). Based on prior study of FeSi, many Mn $3d$ bands near the Fermi level should be expected, together with the occurrence of several valence and conduction band extrema within a few tens of meV of the Fermi level.

We have presented a detailed look at the electronic structure of MnSi both in its paramagnetic phase, which is relevant to the quantum critical point, and also for the FM phase with the observed value of the magnetization. Peculiarities arising from the nonsymmorphic nature of the space group are evident. One peculiarity is the sticking together in pairs of bands over the *entire surface* of the Brillouin zone. This sticking allows a related uncommon feature: the Fermi surfaces contact the BZ face at other than a right angle. This is done in pairs, and one result is that there is a much larger phase space available for $q \rightarrow 0, \omega \rightarrow 0$ interband transitions than would be the case without band sticking. Such transitions occur only for intersecting Fermi surfaces; one may say that the B20 space group strongly encourages intersecting Fermi surfaces (on the BZ faces). Such transitions may be responsible for the unconventional temperature dependence of resistivity and frequency dependence of the optical conductivity. These questions will be pursued in more detail elsewhere.

The space group also leads to some nonzero velocities at the zone center as well as on the BZ faces (these latter related again to the band sticking). The latter occurrence arises in the threefold degenerate states at $k=0$: one has vanishing velocity, while the other two have velocities that are equal in magnitude and different in sign. This phenomenon obtains importance because one such level lies precisely at E_F for the case of FM order. Such an occurrence also marks a point of change of topology of the Fermi surface, which carries with it in principle a Lifshitz transition of order $\frac{5}{2}$.[31–34]

There is also the feature of saddle points or other points of vanishing velocity in the bands falling at E_F. For zero magnetization this occurs at the zone face X point, and also an M point saddle point is close to E_F. For the FM case, a vanishing velocity at a fourfold degenerate state at R lies within 30 meV of E_F. Almost exactly at E_F at the zone center is a threefold level, where the anomalous feature is not the zero velocity (usual at $k=0$) but rather the two nonvanishing velocities. A near (but not exact) occurrence of nonvanishing velocities at $k=0$ (which can be interpreted as diverging effective mass) has been studied in the skutterudite materials.[37] Such band features definitely influence the spectrum of low-energy excitations of the system, and may help to account for the observed peculiarities in the normal state properties of MnSi.

The lack of inversion symmetry *per se* has not been implicated in the peculiarities we have located, partly because time-reversal symmetry restores the band symmetry (and band sticking) that "normally" would be provided by inversion. Affects of the lack of inversion will arise in the FM phase when spin-orbit coupling is considered, in which case (1) some of the band sticking will be relieved and (2) there is no longer enough symmetry to enforce $\varepsilon_{-k}=\varepsilon_k$. One important result is that the Fermi surface becomes "lopsided," restricting the formation of zero-momentum superconducting pairs built from $\vec{k}$ and $-\vec{k}$. We will pursue this question elsewhere; however, spin-orbit coupling is small in Mn so its importance will have to be assessed.

VI. CONCLUSIONS

MnSi is attracting great attention due to its quantum critical point under modest pressure and to the unusual behavior of several normal state properties in the general vicinity of the quantum critical point. We have provided a detailed analysis of the effects of the B20 crystal structure—both the nonsymmorphic space group without a center of inversion and the unusual coordination—on the band structure of both the paramagnetic and ferromagnetic phases. Several types of unusual occurrences have been identified, and some of them are likely to be implicated in the anomalous normal state behavior and possibly the lack of any superconducting phase in the vicinity of the quantum critical point.

ACKNOWLEDGMENTS

We acknowledge illuminating discussions with J. Kuneš, I. I. Mazin, and C. Pfleiderer, and important technical assistance from D. Kasinathan and K.-W. Lee. W.E.P. acknowledges illuminating communication on the band sticking question with J. Kuneš and N. D. Mermin. This work was supported by DOE Grant No. DE-FG03-01ER45876.

[1] L. F. Mattheiss and D. R. Hamann, Phys. Rev. B **47**, 13 114 (1993).

[2] J. H. Wernick, G. K. Wertheim, and R. C. Sherwood, Mater. Res. Bull. **7**, 1431 (1972).

[3] Y. Ishikawa, K. Tajima, P. Bloch, and M. Roth, Solid State Commun. **19**, 525 (1976).

[4] G. Shirane, R. Cowley, C. Majkrzak, J. B. Sokoloff, P. Pagonis, C. H. Perry, and Y. Ishikawa, Phys. Rev. B **28**, 6251 (1983).

[5] P. Bak and M. H. Jensen, J. Phys. C **13**, L881 (1980).

[6] C. Thessieu, J. Flouquet, G. Lapertot, A. N. Stepanov, and D. Jaccard, Solid State Commun. **95**, 707 (1995).

[7] C. Pfleiderer, G. J. McMullan, S. R. Julian, and G. G. Lonzarich,

Phys. Rev. B **55**, 8330 (1997).
[8] C. Thessieu, C. Pfleiderer,A. N. Stepanov, and J. Floquet, J. Phys.: Condens. Matter **9**, 6677 (1997).
[9] N. Doiron-Leyraud, I. R. Walker, L. Taillefer, M. J. Steiner, S. R. Julian, and G. G. Lonzarich, Nature (London) **425**, 595 (2003).
[10] W. Yu, F. Zamborszky,J. D. Thompson, J. L. Sarrao, M. E. Torelli, Z. Fisk, and S. E. Brown, Phys. Rev. Lett. **92**, 086403 (2004).
[11] C. Thessieu, K. Ishida, Y. Kitaoka, K. Asayama, and G. Lapertot, J. Magn. Magn. Mater. **177–181**, 609 (1998).
[12] I. M. Gat-Malureanu, A. Fukaya, M. I. Larkin, A. J. Millis, P. L. Russo, A. T. Savici, Y. J. Uemura, P. P. Kyriakou, G. M. Luke, C. R. Wiebe, Y. V. Sushko, R. H. Heffner, D. E. MacLaughlin, D. Andreica, and G. M. Kalvius, Phys. Rev. Lett. **90**, 157201 (2003).
[13] F. P. Mena, D. van der Marel, A. Damascelli, M. Fäth, A. A. Menovksy, and J. A. Mydosh, Phys. Rev. B **67**, 241101 (2003).
[14] B. Roessli, P. Böni, W. E. Fischer, and Y. Endoh, Phys. Rev. Lett. **88**, 237204 (2002).
[15] O. Nakanishi, A. Yanase, andA. Hasegawa, J. Magn. Magn. Mater. **15–18**, 879 (1980).
[16] L. Taillefer, G. G. Lonzarich, and P. Strange, J. Magn. Magn. Mater. **54–57**, 957 (1986).
[17] Y. Imai, M. Mukaida, K. Kobayashi, and T. Tsunoda, Intermetallics **9**, 261 (2001).
[18] H. Yamada and K. Terao, Phys. Rev. B **59**, 9342 (1999).
[19] H. Yamada, K. Terao, and H. Morozumi, Physica B **294–295**, 141 (2001).
[20] P. Lerch and T. Jarlborg, J. Magn. Magn. Mater. **131**, 321 (1994).
[21] L. Vočadlo, G. D. Price, and I. G. Wood, Acta Crystallogr., Sect. B: Struct. Sci. **55**, 484 (1999).
[22] V. E. Dmitrienko, Acta Crystallogr., Sect. A: Found. Crystallogr. **50**, 515 (1994).
[23] G. Kresse and J. Furthmüller, Phys. Rev. B **54**, 11 169 (1996).
[24] K. Koepernik and H. Eschrig, Phys. Rev. B **59**, 1743 (1999); H. Eschrig, *Optimized LCAO Method and the Electronic Structure of Extended Systems* (Springer, Berlin, 1989).
[25] J. P. Perdew and Y. Wang, Phys. Rev. B **45**, 13 244 (1992).
[26] A. König and N. D. Mermin, Proc. Natl. Acad. Sci. U.S.A. **96**, 3502 (1999).
[27] A. König and N. D. Mermin, Am. J. Phys. **68**, 525 (2000).
[28] Z. Szotek, B. L. Gyorffy, W. M. Temmerman, and O. K. Andersen, Phys. Rev. B **58**, 522 (1998).
[29] D. M. Newns, C. C. Tsuei, R. P. Huebener, P. J. M. van Bentum, P. C. Pattnaik, and C. C. Chi, Phys. Rev. Lett. **73**, 1695 (1994).
[30] T. Takahashi, T. Yokoya, A. Chainani, H. Ding, J. C. Campuzano, M. Kasai, and Y. Tokura, Physica C **282–287**, 218 (1997).
[31] I. M. Lifshitz, Zh. Eksp. Teor. Fiz. **38**, 1569 (1960) [Sov. Phys. JETP **11**, 1130 (1960)].
[32] L. Dagens, J. Phys. (Paris), Lett. **37**, L37 (1970); L. Dagens, J. Phys. F: Met. Phys. **8**, 2093 (1978).
[33] W. E. Pickett, A. J. Freeman, and D. D. Koelling, Phys. Rev. B **22**, 2695 (1980).
[34] A. K. McMahan, Phys. Rev. B **17**, 1521 (1978).
[35] W. E. Pickett, H. Krakauer, and R. E. Cohen, Physica B **165**, 1055 (1990).
[36] P. Frigeri, D. F. Agterberg, A. Koga, and M. Sigrist, Phys. Rev. Lett. **92**, 097001 (2004).
[37] D. J. Singh and W. E. Pickett, Phys. Rev. B **50**, 11 235 (1994).